Journal of Hydroscience and Hydraulic Engineering
Vol. 13, No. 1, May, 1995, 35-45

LATERAL BED-LOAD TRANSPORT AND SAND-RIGDE FORMATION NEAR VEGETATION ZONE IN AN OPEN CHANNEL

By

Tetsuro TSUJIMOTO

Associate Professor, Department of Civil Engineering, Kanazawa University
2-40-20, Kodatsuno, Kanazawa, 920, Japan

and

Tadanori KITAMURA

Research Assistant, School of Global Environmental Engineering, Kyoto University
Yoshida Honmachi, Sakyo-ku, Kyoto, 606, Japan

ABSTRACT

In an open channel with vegetation zone, an organized motion accompanying the water-surface fluctuation takes place and it contributes the lateral mixing. Such an organized motion is in low-frequency and in phase along the depth, it causes lateral component of the bed-load transport as well as suspended sediment, which fluctuates and the net component appears. After modeling the flow properties based on the experimental results, the alternate transport of bed load in the lateral direction is described with non-equilibrium transport model to explain the sand ridge formation along the interface of the vegetation zone.

INTRODUCTION

Recently river improvement projects must meet the desire of the people for more natural environment, and some vegetation areas are preserved in rivers. Some plants often form longitudinally continuous zones of vegetation (for example, bushes of willow), and such vegetation zones often provide ecologically or environmentally favorable spaces. During floods in such a river with vegetation zone, the water flows even in the vegetation area, and it influences the flow in the main water-course. It causes the lateral mixing due to coexistence of the faster flow in the main channel and the slower flow in the vegetation zone neighboring to each other. The momentum exchange brings about the increase of the resistance, and the lateral flux of mass or the sediment brings about river morphological change. In particular, the deposition of sediment in the vegetation zones promotes the growth of the vegetation areas. In this study, the flow and the sediment transport in a channel with vegetation zone are fundamentally studied with particular reference to the organized fluctuation with low frequency. A quasi-uniform flow with depth smaller than the vegetation height with bed-load transport is treated in order to extract the basic mechanism.

By laboratory experiments, Fukuoka & Fujita (4) and Tsujimoto & Kitamura (7, 8, 11) found an appreciable water-surface fluctuation, and an organized motion related to this water-surface fluctuation was focused on. Chu et al. (1) and Ikeda & Ohta (3) tried to explain the appearance of such an organized motion as an instability of horizontal shear flow; while Tsujimoto & Kitamura (9) as an instability of an interrelating system constituted by the water-surface fluctuation and the lateral velocity fluctuation.

In this paper, the following idealized situation (see Fig.1) is treated: The vegetation is idealized as group of cylinders with a constant diameter set on the bed at the equi-spacing, and the zone along the side wall of the channel is to be vegetated. When the whole bed is covered by the vegetation and the flow depth is smaller than the vegetation height, the characteristic velocity U_{s0} appears in the vegetation zone and it is written as

$$U_{s0} = K_s\sqrt{I} \tag{1}$$

K_S represents the hydraulic characteristics of the vegetation layer, and I=energy gradient. When the group of cylinders represents the vegetation, K_S is given by

$$K_S = \sqrt{\frac{2gs^2}{C_D D}} \qquad (2)$$

in which C_D=drag coefficient; D=diameter of cylinders; s=interval between the centers of cylinders; and g=gravity acceleration.

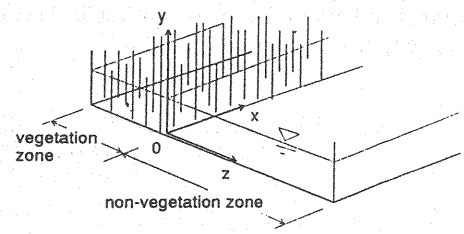

Fig.1 Model channel with vegetation zone

OPEN-CHANNEL FLOW WITH LONGITUDINAL ZONE OF VEGETATION

Characteristics of Flow with Vegetation Zone in Laboratory Flume

Quasi-uniform flow with the depth smaller than the vegetation height in the idealized channel illustrated in Fig.1 was studied experimentally. The experiments were conducted in two flumes. One was 12m long and 0.4m wide (flume-a), and another was 12m long and 0.5m wide (flume-b). The K_S values of the model vegetation were as follows: A: K_S=295cm/s, B: K_S=234cm/s, C: K_S=120cm/s, and D: K_S=137cm/s, E: K_S=172cm/s. The properties of model vegetation are shown in Table 1. Model vegetation A, B and C were set in the flume-a, and D and E were set in the flume-b. The experimental conditions are summarized in Table 2, in which B_S=width of vegetation zone; i_b=longitudinal bed slope; h_0=mean water depth; U_{ave}=bulk velocity; U_k=velocity at the interface between vegetation and non-vegetation zones (depth-averaged); C_f=resistance coefficient of main course and $\Omega \equiv C_D D h_0/(2s^2)$. The velocity measurements were conducted by a micro-propeller currentmeter and a small electromagnetic currentmeter in the flume-a, and a hot-film anemometer in the flume-b. The water-surface fluctuation was measured by capacity limnimeters. The outputs from the instruments were recorded to floppy disks (sampling frequency: 20Hz, number of samples: 1,024), and they were statistically processed by a computer.

Table 1 Properties of model vegetation

model	quality of material	diameter D (cm)	height K (cm)	spacing s (cm)	number of cylinder at one point	K_S (cm/s)
A	bamboo	0.15	4.6	2.8	1	295
B	bamboo	0.15	4.6	2.0	1	234
C	vinyl chloride	0.02	5.0	1.0	4	120
D	6-6 nylon	0.1	4.1	1.0	1	137
E	bamboo	0.25	10.0	2.0	1	172

Table 2 Experimental condition

RUN	Flume	B_S (cm)	i_b ($\times 10^{-3}$)	h_0 (cm)	U_{ave} (cm/s)	U_k (cm/s)	C_f ($\times 10^{-3}$)	Ω	measu-rement
A1	a	12	1.70	4.57	32.0	20.1	3.8	0.050	P,E
B1	a	12	1.70	4.28	27.6	16.3	4.0	0.116	P,E
B2	a	12	1.74	3.22	23.7	14.1	4.5	0.087	P
B3	a	12	2.68	4.15	35.1	18.5	3.6	0.112	P,E
B4	a	6	1.64	4.23	33.9	14.4	3.5	0.114	P,E
C1	a	12	1.65	4.38	22.0	10.5	5.2	0.298	P,E
D1	b	25	1.49	3.65	20.3	13.5	3.1	0.183	H
D2	b	25	2.50	3.82	24.2	16.1	4.2	0.191	H
D3	b	25	3.87	3.87	27.8	16.8	3.4	0.194	H
E1	b	25	10.0	4.10	39.0	28.0	9.1	0.136	H

#P:micro-propeller currentmeter
E:electromagnetic anemometer
H:hot film anemometer

Figure 2 shows the lateral distributions of the velocity (U), the standard deviations of longitudinal and lateral velocities (u_{rms} and w_{rms}), the Reynolds stress in the lateral direction ($-\overline{uw}$), and the standard deviation of water-surface elevation (h_{rms}). From these figures, one can recognize the transitional zone (interfering zone) where the lateral gradient of velocity, the turbulence intensity, the Reynolds stress in the lateral direction and the variance of the water-surface fluctuation show high values.

Simultaneous measurements were conducted with an electromagnetic currentmeter and a limnimeter as shown in Fig.3, and we obtained time series of the water-surface elevation $h'(t)$, and the longitudinal and lateral components of velocity, $u(t)$ and $w(t)$, as shown in Fig.4. The fluctuations are rather regular and in low frequency. The dominant period is a few second. And, they are strongly correlated to each other. We can recognize obvious phase shifts among them as shown in Fig.5. Simultaneous measurements of the water-surface fluctuations at two different points in the same cross-section were also conducted with two limnimeters, which clarified that the fluctuations in the same cross-section are in phase as shown in Fig.6. Simultaneous measurements were conducted also at two different points on the longitudinal axis, which clarified that the fluctuation is rather convective with the propagation celerity almost equal to the flow velocity near the interface between vegetation and non-vegetation zones, as suggested by a strong cross-correlation and the temporal shift of the peak of the cross-correlation coefficient in Fig.7. Furthermore, simultaneous measurements of the water-surface and local velocity were conducted, and it clarified that the correlative characteristics among them

(correlation coefficient and phase shift) hardly vary along the depth. It suggests that low-frequency organized fluctuation is still effective near the bed.

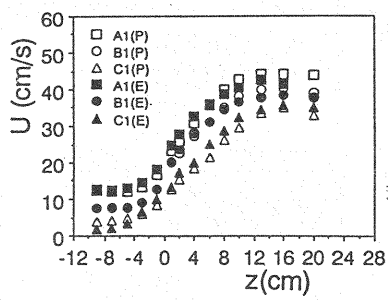

Fig.2(a) Lateral distribution of mean primary velocity

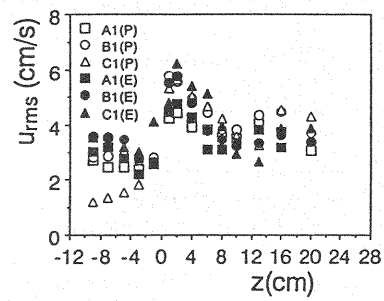

Fig.2(b) Longitudinal turbulence intensity

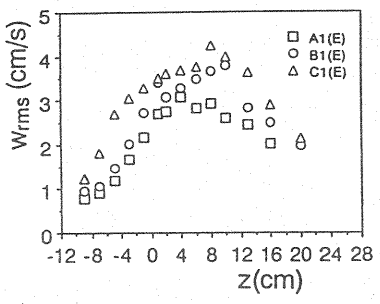

Fig.2(c) Lateral turbulence intensity

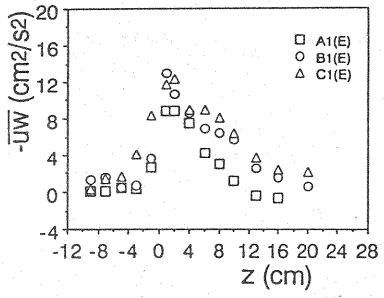

Fig.2(d) Reynolds stress in lateral direction

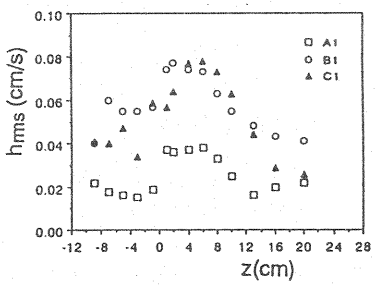

Fig.2(e) R.M.S. of water-surface fluctuation

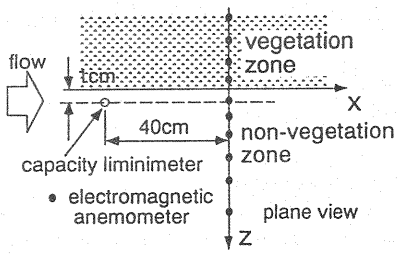

Fig.3 Simultaneous measurements of velocity and water-surface fluctuation

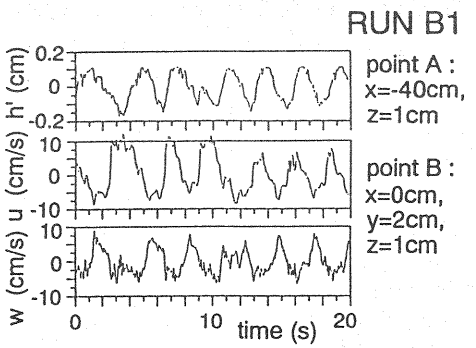

Fig.4 Time series of h', u and w

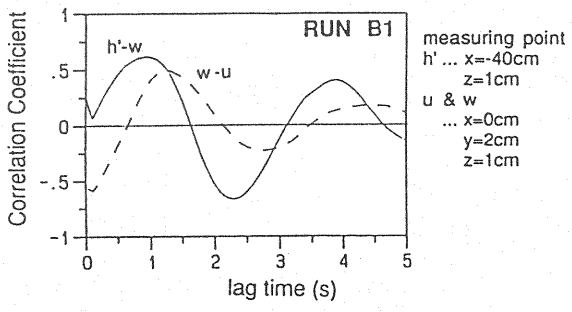

Fig.5 Cross-correlations among h', u and w

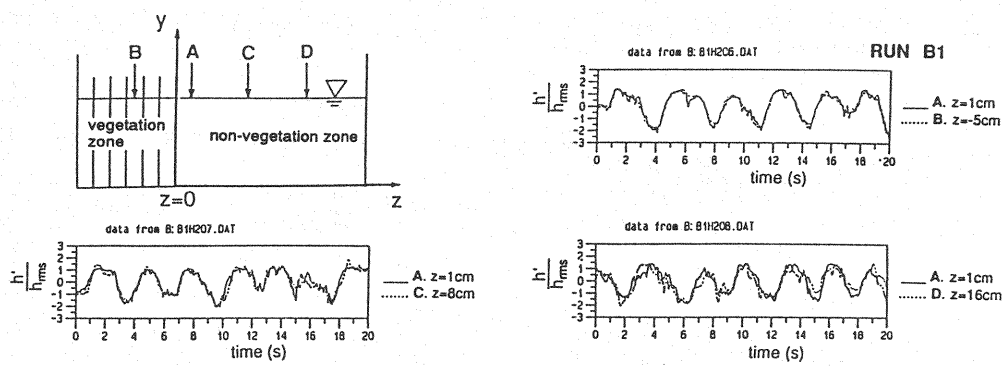

Fig.6 Normalized time series of h' at different points in same cross section

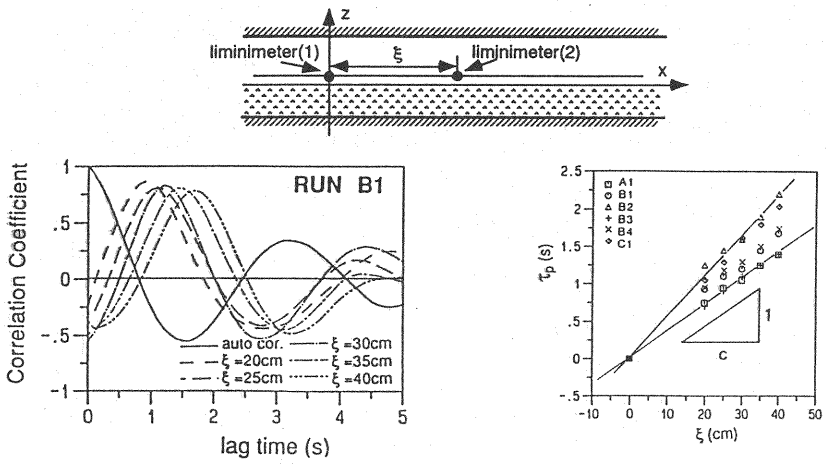

Fig.7 Time-space correlation of water-surface fluctuation and its propagation

The results as shown in Fig.5 are arranged as Fig.8, where the cross-correlation between h' and w, ψ_{hw}, and that between w and u, ψ_{wu} are plotted against the lateral coordinate. According to this figure: ψ_{hw} is around $3\pi/2$ through the cross section; ψ_{wu} is around $\pi/2$ in the vegetation zone and $3\pi/2$ in the non-vegetation zone, while around π in the interaction zone between vegetation and non-vegetation zones. The relation $\psi_{wu}=\pi$ implies the most efficient exchange of momentum. One can conclude that the momentum exchange near the boundary of the vegetation zone is mainly contributed to by two-dimensional organized motion in low frequency associated with the water-surface fluctuation.

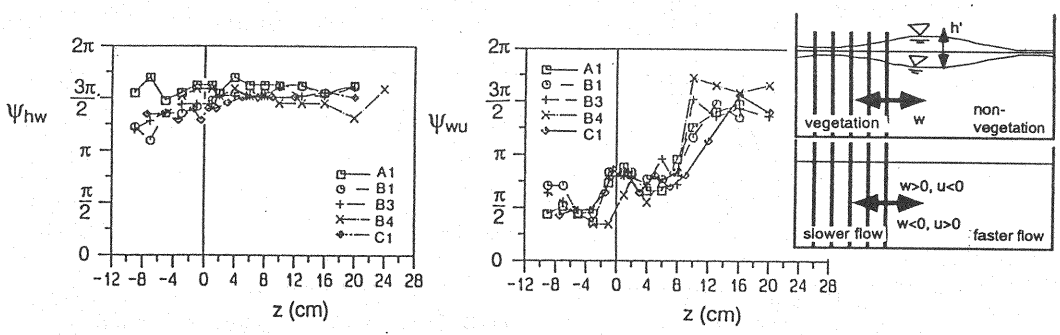

Fig.8 Phase shift of w to h' and that of u to w

Simplified Description of Flow with Vegetation

Based on the flume experiments (see Fig.2(a)), the following exponential-type distribution is adopted for $U(z)$, which is deduced from an analysis of a horizontal shear flow with a constant eddy viscosity.

$$U^{\#} = 1 + \left(\sqrt{\gamma} - 1\right)\exp\left(-\frac{z}{b_m}\right) \quad (z \geq 0) \; ; \quad U^{\#} = \gamma + \left(\sqrt{\gamma} - \gamma\right)\exp\left(\frac{z}{b_s}\right) \quad (z \leq 0) \tag{3}$$

in which

$$\gamma \equiv \frac{U_{s0}}{U_{m0}} = \sqrt{\frac{C_f}{(C_f+\Omega)}} \; ; \quad \frac{b_m}{h_0} = \sqrt{\frac{\varepsilon_{M*}}{2}}\, C_f^{-1/4} \; ; \quad \frac{b_s}{h_0} = \sqrt{\frac{\varepsilon_{M*}}{2}}\, (C_f+\Omega)^{-1/4} \tag{4}$$

in which $U^{\#} \equiv U/U_{m0}$; $U_{m0} \equiv \sqrt{1/C_f} \cdot u_{*0}$=flow velocity in main course unaffected by vegetation zone; C_f=resistance coefficient of main course; $u_{*0} \equiv \sqrt{gh_0 I}$; h_0=mean flow depth; b_m, b_s=effective width of shear flow regions in main course and that in vegetation zone, respectively; $\Omega \equiv C_D D h_0/(2s^2)$; $\varepsilon_{M*} \equiv \varepsilon_M/(u_{*0} h_0)$; and ε_M=kinematic eddy viscosity. Ikeda et al. (2, 3) assumed the following equation to evaluate the kinematic eddy viscosity.

$$\varepsilon_{M*} = \frac{f(1-\gamma)}{\sqrt{C_f}} \frac{(b_m+b_s)}{h_0} \tag{5}$$

in which f is an empirical parameter and is often termed "mixing coefficient." The model expresses the experimental results of the lateral distribution of primary velocity if one chooses the f-value properly. The values of f determined by fitting for the respective velocity profiles are plotted against γ in Fig.9. The solid curve in the figure is an empirical formula by Ikeda et al.(2, 3) written as follows:

$$f = 0.035\exp[-2.95\exp(-3.8\gamma)] \tag{6}$$

When the shear flow regions in the main course and the vegetation zone are respectively one-dimensionalized and the lateral velocity fluctuation at the interface (z=0) is approximated by a sinusoidal wave with the amplitude w_0, the interfacial shear between the main course and the vegetation zone, τ_{int}, is given by averaging the lateral momentum flux during one period of fluctuation as follows:

$$\frac{\tau_{int}}{\rho} = \frac{w_0(U_m - U_s)}{\pi} = \frac{1-\gamma}{e\pi} w_0 U_{m0} \tag{7}$$

in which U_m, U_s=mean velocities of the mixing zone in the main course and the vegetation zone, respectively; and Eq.3 has been applied to obtain the right hand side of Eq.7. On the other hand, $\tau_{int} = \rho \varepsilon_M \cdot dU/dz\,|_{z=0}$, and substitution of Eqs.3 and 6 into it also gives an expression of τ_{int}. Comparing it with Eq.7, one obtains the following relation between f and w_0:

$$w_0/U_{m0} = \pi e(1-\gamma) \cdot f \tag{8}$$

One can expect that $w_0 \cong w_{rms}(0)$. The amplitude w_0 estimated by Eqs.8 and 6 is well consistent to $w_{rms}(0)$ obtained experimentally as shown in Fig.10. Moreover, Fig.11 demonstrates the applicability of Eq.8.

The lateral distribution of w_{rms} is approximated by the following equations according to the experimental results.

$$w_{rms}(z) = \begin{cases} w_{rms\infty} + [w_{rms}(0) - w_{rms\infty}] \cdot \exp[-(z/b_m)^2] & (z \geq 0) \\ w_{rms}(0) \cdot \exp[-(z/b_s)^2] & (z \leq 0) \end{cases} \tag{9}$$

in which $w_{rms\infty}$=the value of w_{rms} in main course unaffected by vegetation ($w_{rms\infty}\cong\sqrt{C_f}U_{m0}$).

Based on the above-mentioned scenario is employed where only Eq.6 has been assumed, the depth-averaged flow characteristics are described when the parameters C_f and Ω are given.

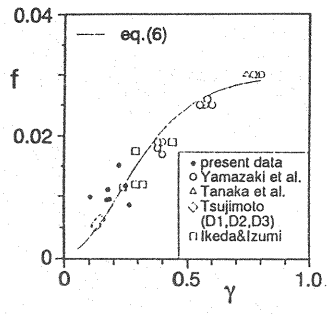

Fig.9 Relation between f & γ

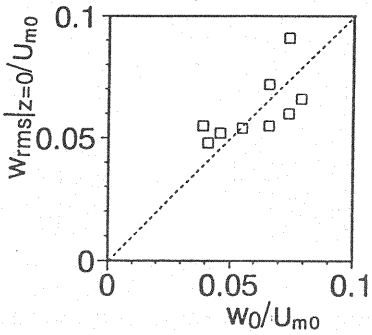

Fig.10 Relation between w_0 and w_{rms}

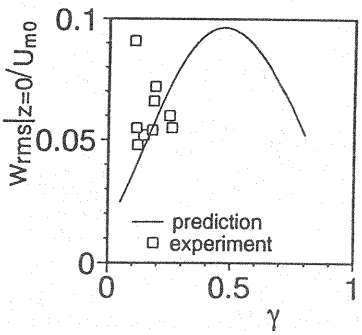

Fig.11 Relation between w_{rms} and γ

BED-LOAD MOTION NEAR THE INTERFACE BETWEEN VEGETATION AND NON-VEGETATION ZONES AND SAND RIDGE FORMATION

Simplified Description of Bed-Load Transport near Vegetation Zone

The lateral velocity fluctuation (w) is here approximated as an alternation of w_{rms} and $-w_{rms}$ as shown in Fig.12, and subsequently, the trajectory of a bed-load particle changes with a deflection angle ϕ_1 and ϕ_2 against the x axis (the subscripts 1 and 2 imply the values during $w>0$ and $w<0$, respectively). During one period of the low-frequency fluctuation, ΔT_L, $w>0$ during one half period of it, and $w<0$ during the other half of it. When the non-equilibrium bed-load transport model proposed by Nakagawa & Tsujimoto (5) is applied along the trajectory of bed-load motion, the amount of sediment, $q_{Bzj}\Delta T_L/2$, given by the following equation is transported laterally during each half period:

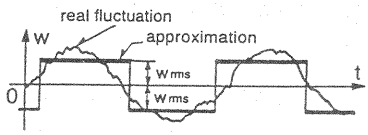

Fig.12 Model for w(t)

$$q_{Bzj}(z)\cdot\frac{\Delta T_L}{2}=-(-1)^j\frac{A_3 d}{A_2}\int_0^\infty p_s(z+(-1)^j\zeta)\cdot\exp\left[-\frac{\zeta}{\Lambda\sin|\phi_j(z)|}\right]d\zeta\,\frac{\Delta T_L}{2} \tag{10}$$

in which q_{Bzj}=lateral component of the non-equilibrium bed-load transport rate during each half period; j=subscript to represent the sign of w ($w>0$ for $j=1$; $w<0$ for $j=2$); A_2, A_3=two- and three-dimensional geometrical coefficients for sand; d=sediment diameter; p_s=pick-up rate (probability density per unit time for a sand particle to be dislodged); Λ=step length of bed-load motion; and it has been assumed that the step length follows an exponential distribution. Because the pick-up rate at $z-\zeta$ and that at $z+\zeta$ are different from each other, $q_{Bz1}(z)$ and $q_{Bz2}(z)$ are not necessarily in balance even if $|\phi_1(z)|=|\phi_2(z)|$. The net lateral transport rate of bed load, $q_{Bz}^{net}(z)$, is given as follows:

$$q_{Bz}^{net}(z)\Delta T_L=q_{Bz1}(z)\cdot\frac{\Delta T_L}{2}+q_{Bz2}(z)\cdot\frac{\Delta T_L}{2} \tag{11}$$

$$q_{Bz}^{net}(z)=\frac{A_3 d}{2A_2}\int_0^\infty\left\{p_s(z-\zeta)\exp\left[-\frac{\zeta}{\Lambda\sin|\phi_1(z)|}\right]-p_s(z+\zeta)\exp\left[-\frac{\zeta}{\Lambda\sin|\phi_2(z)|}\right]\right\}d\zeta \tag{12}$$

When the lateral bed slope is not large, the direction of bed-load motion is related to the flow direction β and the lateral bed slope θ, as follows (Nakagawa et al.(6)).

$$\tan\phi \equiv \frac{\tan\theta}{\sqrt{\mu_d T^*}} + \tan\beta \tag{13}$$

in which $T^* \equiv \mu_d \tau_* / \tau_{*c}$; μ_d=friction coefficient of sand; $\tau_* \equiv u_*^2/[(\sigma/\rho-1)gd]$; u_*=shear velocity; σ, ρ=mass densities of sand and water, respectively; and τ_{*c}=dimensionless critical tractive force.

In case of flat bed, $\phi(z) \equiv |\phi_1(z)| = |\phi_2(z)|$ because the direction of bed-load motion follows the flow direction, and thus, Eq.12 is rewritten as

$$q_{Bz}^{net}(z) = \frac{A_3 d}{2A_2}\int_0^\infty \left[p_s(z-\zeta) - p_s(z+\zeta)\right]\exp\left\{-\frac{\zeta}{\Lambda\sin[\phi(z)]}\right\}d\zeta \tag{14}$$

The pick-up rate p_s in Eq.12 is expressed as Taylor's expansion with respect to ζ as follows:

$$p_s(z+(-1)^j\zeta) = p_s(z) + (-1)^j\zeta\frac{\partial p_s}{\partial z} + \frac{\zeta^2}{2}\frac{\partial^2 p_s}{\partial z^2} + \cdots\cdots \tag{15}$$

When the bed shear stress is larger than the critical tractive force and the lateral change of p_s is approximated in a linear form, the higher order terms of ζ is neglected, and substituting Eq.15 into Eq.14 leads the following simple expression.

$$q_{Bz}^{net}(z) = -\frac{A_3\Lambda^2 d}{A_2}\frac{\partial p_s}{\partial z}\cdot\sin^2[\phi(z)] \tag{16}$$

This is a rough expression but one can easily understand the fact that there is a net flux of bed-load toward the vegetation zone to form the lateral bed slope. The lateral bed slope suppresses the lateral bed-load flux according to Eq.13 and the lateral bed profile reaches an equilibrium. Under ordinary conditions, the net transport rate of lateral bed-load motion should be calculated based on Eq.12 directly with aid of numerical method.

Calculated Results of Lateral Bed-Load Transport

Based on the model of this paper, the net flux of lateral bed-load transport is calculated. The conditions are as follows: The vegetation layer is characterized by the parameter Ω; the bed materials by d and σ/ρ; and the hydraulic condition by the undisturbed Froude number, $Fr_0 \equiv U_{m0}/\sqrt{gh_0}$ and the relative roughness, d/h_0. When a flat bed is considered, Manning-Strickler's equation is applied to estimate C_f from Fr_0 and d/h_0. The direction of bed-load motion on a flat bed is given as follows: $\sin\phi(z) \equiv w_{rms}(z)/[U(z)]$, where Eqs.3 and 9 are applied to estimate $U(z)$ and $w_{rms}(z)$. The shear velocity, $u_*(z)$, is estimated from $U(z)$ by assuming that C_f is constant, and the dimensionless bed shear stress, τ_*, is evaluated as follows:

$$\tau_{*0} \equiv \frac{u_{*0}^2}{(\sigma/\rho-1)gd} = \frac{C_f Fr_0^2}{(\sigma/\rho-1)(d/h_0)} \tag{17}$$

Then, the pick-up rate is estimated by using Nakagawa-Tsujimoto formula (5), which is written as follows:

$$\frac{p_s}{\sqrt{(\sigma/\rho-1)g/d}} = 0.03\tau_*\left(1-\frac{0.7\tau_{*c}}{\tau_*}\right)^3 \tag{18}$$

While, the mean step length is assumed to be 100 times sand diameter.

Figure 13 shows the calculated examples of net lateral transport rate of bed load with changing the parameters, Fr_0, d/h_0 and Ω, where the solid curves correspond to the results obtained directly by Eq.12 with the aid of numerical method while the dashed curve to an approximation by Eq.16. The graph is depicted in the dimensionless forms, where $q_{Bz\#}^{net} \equiv q_{Bz}^{net}/q_{B0}$; $q_{B0}=(A_3/A_2)p_{s0}\Lambda d$=longitudinal bed-load transport rate in the main course unaffected by the vegetation; and $z_\# \equiv z/h_0$. Eq.16 cannot provide an accurate result where the bed shear is near the critical tractive force.

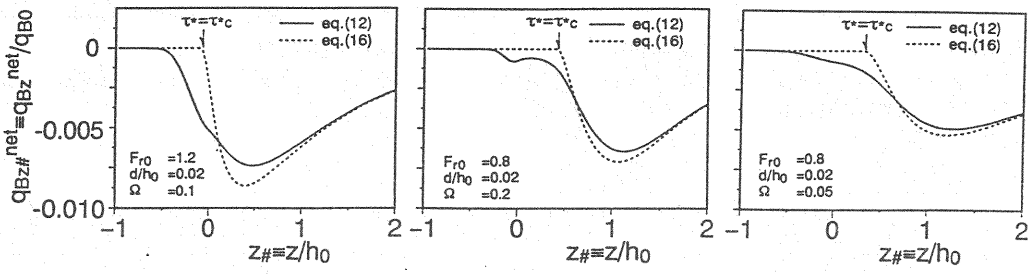

Fig.13 Calculated net lateral transport rate of bed-load

Comparison with Flume Experiments

Movable bed experiments with uniform sand were conducted in the laboratory flume (flume-b with model vegetation-E), where Ω=0.157; Fr_0=1.44; and d/h_0=0.021 (d=0.088cm, h_0=4.1cm, D=0.25cm, s=2cm, K_s=172cm/s). The movable bed was initially flattened, and the measurement of the sediment transport was finished before the bed undulation became appreciably large. A sediment trap as illustrated in Fig.14 was devised to measure the lateral flux of bed load for both directions separately. The measured values of net lateral transport rate are plotted in Fig.15 with the calculated curve and it has been verified that the present model can predict the lateral transport rate of bed load with good accuracy.

The bed geometry at 10min after introducing the flow over the initially flattened bed is shown in Photo 1, where a sand ridge parallel to the longitudinal axis near the interface in the vegetation zone is clearly seen. The measured lateral bed profile, $y_b(z)/h_0$, is shown in Fig.16, where the calculated $\partial q_{Bz}^{net}/\partial z$ is also plotted, which is expected to be proportional to $(-\partial y_b/\partial t)$. The observed bed profile is more gradual than the profile estimated from the calculated distribution of $\partial y_b/\partial t$ under the assumption of a flat bed. It is caused by the change of the direction of bed-load motion due to the gravity by the lateral bed slope.

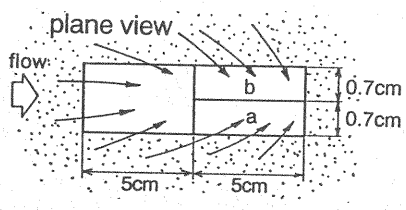

Fig.14 Devised sand trap

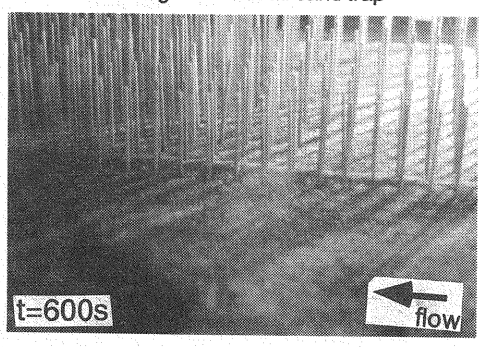

Photo 1 Longitudinal sand ridge

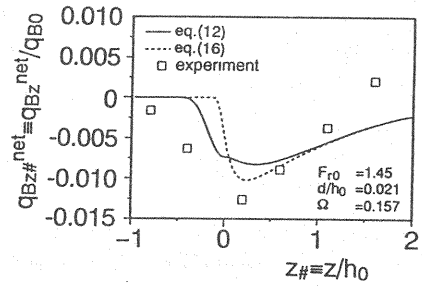

Fig.15 Measured net lateral bed-load transport rate

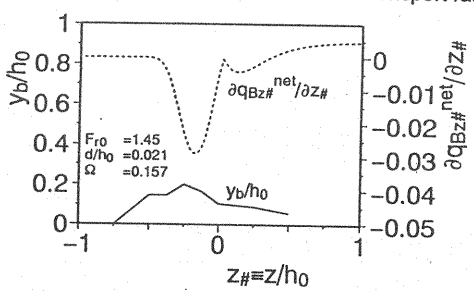

Fig.16 Lateral bed profile

CONCLUSION

The flow near the interface between vegetation and non-vegetation zone is characterized by organized fluctuations of the water-surface and the longitudinal and the lateral components of velocity, and such fluctuations contribute to the lateral exchanges of momentum and mass. The frequency of such fluctuations are so low and the lateral velocity fluctuation is so intense even near the bottom that it affects bed-load motion. The appearance of net flux of bed load in lateral direction is expected by applying non-equilibrium transport model, and it explains a longitudinal sand ridge formation.

REFERENCES

1. Chu, V.H., J.H. Wu and R.E. Khayat : Stability of lateral shear flows in shallow open channel, *Jour. Hydraul. Eng.*, ASCE, Vol.117, No.10, pp.1370-1388, 1991.
2. Ikeda, S., N. Izumi and R. Ito : Effects of Pile Dikes on Flow Retardation and Sediment Transport, *Jour. Hydraul. Eng.*, ASCE, Vol.117, No.11, pp.1459-1478, 1991.
3. Ikeda, S., K. Ohta : Instability Induced horizontal vortices in shallow open-channel flows, *9th Sym. on Turbulent Shear Flows*, Kyoto, Japan, pp.14-1-1 - 14-1-6, 1993.
4. Fukuoka, S. and K. Fujita : Hydraulic effects of luxuriant vegetations on flood flow, *Rep. Public Works Res. Inst.*, Ministry of Construction, Japan, No.180, pp.129-192, 1988 (in Japanese).
5. Nakagawa, H. and T. Tsujimoto : Sand bed instability due to bed load motion, *Jour. Hydraul. Div.*, ASCE, Vol.106, HY12, pp.2029-2051, 1980.
6. Nakagawa, H., T. Tsujimoto and S. Murakami : Non-equilibrium bed load along side bank, *Proc. 3rd Int. Sym. River Sedimentation*, Jackson, Mississippi, USA, pp.1029-1065, 1986.
7. Tsujimoto, T. : Spectral analysis of velocity and water-surface fluctuations appearing in an open chanel with vegetated and non-vegetated regions in a cross section, *Proc. 6th Int. Sym. Stochastic Hydraulics*, Taipei, R.O.C., pp.197-212, 1992.
8. Tsujimoto, T. and T. Kitamura : Experimental study on open-channel flow with vegetated zone along side wall - Correlative structure of fluctuations of velocity and free surface, *KHL Commun.*, Kanazawa Univ., Vol.3, pp.21-35, 1992.
9. Tsujimoto, T. and T. Kitamura : Appearance of organized fluctuations in open-channel flow with vegetated zone, *KHL Commun.*, Kanazawa Univ., Vol.3, pp.37-45, 1992.
10. Tsujimoto, T., T. Kitamura and H. Nakagawa : Lateral bed-load transport near vegetation zone and formation of flood plain, *Proc. of Hydraulic Engineering*, JSCE, Vol.37, pp.687-692, 1993 (in Japanese).
11. Tsujimoto, T. and T. Kitamura : Experimantal study on mechanism of transverse mixing in ope-channel flow with longitudinal zone of vegetation along side wall, *Proc. JSCE*, No.491, pp.61-70, 1994 (in Japanese).

APPENDIX - NOTATION

The following symbols are used in this paper:

A_2, A_3	= two- and three dimensional geometrical coefficients for sand;
B_s	= width of vegetation zone;
b_m, b_s	= effective width of shear flow regions in main course and that in vegetation zone;
C_D	= drag coefficient of vegetation;
C_f	= resistance coefficient of main course;
D	= diameter of cylinders;
d	= sediment diameter;
F_{r0}	= undisturbed Froude number;
f	= mixing coefficient;
g	= gravity acceleration;
h_0	= mean water depth;
$h'(t)$	= time series of the water-surface elevation;

h_{rms} = standard deviation of water-surface elevation;
I = energy gradient;
i_b = longitudinal bed slope;
K_s = proportionality constant;
p_s = pick-up rate (probability density per unit time for a sand particle to be dislodged);
q_{B0} = longitudinal bed-load transport rate in the main course unaffected by the vegetation zone;
q_{Bz} = lateral component of non-equilibrium bed-load transport rate;
q_{Bz}^{net} = net lateral transport rate of bed-load;
$q_{Bz\#}^{net}$ = dimensionless net lateral transport rate of bed-load;
s = interval between the center of cylinders;
T^* = dimensionless parameter;
t = time;
U = mean primary velocity (depth averaged value);
$U_\#$ = dimensionless mean primary velocity (depth averaged value);
U_{ave} = bulk velocity;
U_k = velocity at the interface between vegetation and non-vegetation zones (depth-averaged)
U_m, U_s = averaged velocities of shear flow region in main course and vegetation zone;
U_{m0} = mean primary velocity in main course unaffected by vegetation zone;
U_{s0} = characteristic velocity in vegetation zone;
u_* = shear velocity;
u_{*0} = friction velocity in main course unaffected by vegetation zone;
$u(t)$, $w(t)$ = time series of longitudinal and lateral components of velocity;
u_{rms}, w_{rms} = standard deviation of longitudinal and lateral components of velocity;
$-uw$ = Reynolds stress in lateral direction (depth averaged value);
w_0 = amplitude of sinusoidal wave;
$w_{rms\infty}$ = depth averaged value of w_{rms} in main course unaffected by vegetation zone;
x, y, z = longitudinal, vertical, lateral coordinates;
y_b = elevation of bed;
$z_\#$ = dimensionless z axis;
β = flow direction;
ΔT_L = period of low frequency fluctuation;
ε_M = kinematic eddy viscosity;
ε_{M^*} = dimensionless kinematic eddy viscosity;
ϕ = deflection angle of trajectory of bed-load particle against x axis;
γ = ratio between characteristic velocity in vegetation zone and mean primary velocity in main course unaffected by vegetation zone;
Λ = mean step length of bed-load motion;

μ_d = friction coefficient of sand;
θ = lateral bed slope;
ρ = mass density of water;
σ = mass density of sand;
τ_p = temporal shift of peak of cross-correlation coefficient;
τ_{int} = interfacial shear stress between main course and vegetation zone;
τ_* = dimensionless tractive force;
τ_{*c} = dimensionless critical tractive force;
τ_{*0} = dimensionless tractive force in main course unaffected by vegetation zone;
Ω = dimensionless vegetation density;
ξ = longitudinal distance of pair of measuring points;
ψ_{hw} = phase shift between $w(t)$ and $h'(t)$;
ψ_{wu} = phase shift between $u(t)$ and $w(t)$;
ψ_{hu} = phase shift between $u(t)$ and $h'(t)$; and
ζ = distance along z axis.

(Received August 15, 1994; revised December 2, 1994)